Physics – Uspekhi **55** (11) 1140 – 1151 (2012)

CONFERENCES AND SYMPOSIA

PACS numbers: 01.10.Fv, 65.80.Ck, 68.65.Pq, 72.15.Jf, 72.20.Pa, 72.80.Vp, 78.67.Wj, 81.05.ue

Physical properties of graphene
(Scientific session of the Physical Sciences Division of the Russian Academy of Sciences, 28 March 2012)

DOI: 10.3367/UFNe.0182.201211h.1223

A scientific session of the Physical Sciences Division of the Russian Academy of Sciences (RAS) devoted to the "Physical properties of graphene" was held on 28 March 2012 in the conference hall of the Lebedev Physical Institute.

The agenda of the session announced on the RAS Physical Sciences Division website www.gpad.ac.ru included the following reports:

(1) **Falkovsky L A** (Landau Institute of Theoretical Physics, RAS, Moscow; Vereshchagin Institute of High-Pressure Physics, RAS, Moscow) "Magnetooptics of graphene";

(2) **Varlamov A A** (The University of Rome Tor Vergata, Italy) "Thermoelectric properties of graphene."

The papers written on the basis of these reports are given below.

PACS numbers: 68.65.Pq, 78.67.Wj, 81.05.ue
DOI: 10.3367/UFNe.0182.201211i.1223

Magnetooptics of graphene layers

L A Falkovsky

1. Introduction

Most of the vast amount of information on graphene can be described based on the concept of "gapless Dirac fermions." According to this concept, at the K points of the Brillouin zone (vertices of a hexagon), there are two zones without a gap between them, and the electron spectrum can be considered linear in a sufficiently wide neighborhood of wave vectors. It is obvious that to assume the spectrum to be linear, the size of the neighborhood under consideration must be small compared to the size of the Brillouin zone, i.e., less than 10^8 cm^{-1}, which suggests not too large concentrations of charge carriers, $n \ll 10^{16}$ cm^{-2}. Ideally pure graphene at zero temperature should contain no charge carriers at all, and the Fermi level should separate the conduction band from the valence band. However, it is quite difficult to prepare pure graphene; the minimum concentration of charge carriers that could be obtained in it to date is $n \sim 10^9$ cm^{-2}. The following key problems arise here: to what extent the Coulomb electron interaction renormalizes the initial linear spectrum and whether graphene can pass into a state with an energy gap.

At present, there is also a practical need in gapped materials for modern electronics. Therefore, investigations of a graphene bilayer to which a constant voltage can be applied (as to a capacitor), thereby creating an energy gap in its spectrum, have become quite popular. In its development over the last half-century, physics has come full circle and returned to the investigation of graphite. Here, we recall the names of Slonczewski and Weiss [1], who formulated the principle of the description of a layered substance with a strong interaction in the layers and a weak interaction between them.

The main methods for studying the metallic state appear to be magnetotransport and magnetooptical investigations. In a magnetic field, phenomena such as Hall effects (classical and quantum) are observed, as is rotation of the polarization plane, or the Faraday effect upon light transmission and the Kerr effect upon reflection. In describing graphene layers, in spite of the relative simplicity of the presented picture, difficulties arise, which, just as the corresponding achievements, are the subject of this paper.

2. Electronic spectrum of graphene

The K points of the Brillouin zone have the C_{3v} symmetry (a 3-fold axis and a symmetry plane). This space group has a two-dimensional representation whose basis is composed of two functions that are transformed into one another under reflection and acquire factors $\exp(\pm 2\pi i/3)$ under rotation. Using the components of the momentum deviation from the K points, linear combinations $k_\pm = \mp i k_x - k_y$ can be composed that transform similarly to the functions of the basis. The effective Hamiltonian must be invariant under a representation of this small group; hence, near the K point, we have a unique possibility of writing the Hamiltonian in the linear approximation:

$$H(\mathbf{k}) = \begin{pmatrix} 0 & vk_+ \\ vk_- & 0 \end{pmatrix}, \qquad (1)$$

L A Falkovsky Landau Institute of Theoretical Physics, Russian Academy of Sciences, Moscow, Russian Federation; Vereshchagin Institute of High-Pressure Physics, Russian Academy of Sciences, Moscow, Russian Federation
E-mail: falk@itp.ac.ru

Uspekhi Fizicheskikh Nauk **182** (11) 1223 – 1234 (2012)
DOI: 10.3367/UFNr.0182.201211h.1223
Translated by S N Gorin; edited by A M Semikhatov

Uspekhi Fizicheskikh Nauk **182** (11) 1223 – 1229 (2012)
DOI: 10.3367/UFNr.0182.201211i.1223
Translated by S N Gorin; edited A M Semikhatov

where v is a constant with the dimension of velocity. The same Hamiltonian is obtained, naturally, in the tight-binding approximation.

The eigenvalues of the matrix in the right-hand side of Eqn (1) give a two-band gapless spectrum:

$$\varepsilon_{1,2} = \mp v\sqrt{k_x^2 + k_y^2} = \mp vk\,.$$

Hence, the gapless character of the spectrum is a mere consequence of the symmetry, and the fact that the Fermi level should pass through the conical point K follows merely from the valence of carbon. The cyclotron mass for such a spectrum is given by

$$m(\varepsilon) = \frac{1}{2\pi}\,\frac{\mathrm{d}S(\varepsilon)}{\mathrm{d}\varepsilon} = \frac{\varepsilon}{v^2}\,,$$

where S is the area of the cross section of the isoenergy surface and the concentration of charge carriers at zero temperature is expressed through the chemical potential μ as

$$n(\mu) = \frac{\mu^2}{\pi\hbar^2 v^2}\,.$$

The simplest way to experimentally verify the type of spectrum is by using the relation

$$m(\mu)\,\frac{v}{\hbar} = \mp\sqrt{\pi n(\mu)}\,,$$

for example, by measuring the Shubnikov–de Haas effect, in which case the cyclotron mass at the Fermi level is found from the temperature dependence of the amplitude of oscillations and the concentration of charge carriers is determined from their frequency. Both these quantities are measured at different concentrations of charge carriers, which is changed by varying the voltage at the ''gate.'' Such a verification was performed by Ellis et al. [2], who obtained very pure samples with a charge-carrier concentration as low as 10^9 cm^{-2}. It turned out that the ''constant'' parameter v is not constant but increases at small concentrations by a factor of three compared to its ''normal'' value 10^8 cm s^{-1} at concentrations exceeding 10^{11} cm^{-2}. This effect is a result of the electron–electron Coulomb interaction, which proves to be more efficient, as was to be expected, at small concentrations, when no screening is observed. The logarithmic renormalization of the velocity due to the Coulomb interaction in the three-dimensional case was first found in [3], and for two-dimensional graphene, in [4]. Interestingly, even at a quite low concentration, no signs of any phase transition have been found. In accordance with the theory, the Coulomb interaction does not violate the symmetry-related gapless character of the spectrum.

3. Dynamic conductivity of graphene

One of the clearest manifestations of the specific character of the graphene spectrum can be provided by the behavior of its dynamic (i.e., frequency-dependent) conductivity (conductance). At higher frequencies, in the optical range, the spatial dispersion of conductivity and the frequency of collisions of charge carriers are insignificant. Summing the contributions from conical points (two per unit cell), integrating over the angle of the two-dimensional vector $\mathbf{k}$, and passing to the variable $\varepsilon = vk$, we find the conductivity as [5–7]

$$\sigma(\omega) = \frac{e^2\omega}{\mathrm{i}\pi\hbar}\left[\int_{-\infty}^{+\infty}\mathrm{d}\varepsilon\,\frac{|\varepsilon|}{\omega^2}\,\frac{\mathrm{d}f(\varepsilon)}{\mathrm{d}\varepsilon} - \int_0^{+\infty}\mathrm{d}\varepsilon\,\frac{f(-\varepsilon)-f(\varepsilon)}{(\omega+\mathrm{i}\delta)^2-4\varepsilon^2}\right], \tag{2}$$

where $f(\varepsilon)$ is the distribution function and δ is an infinitesimal parameter. The first term in the right-hand side of Eqn (2), which represents the intraband contribution, can be integrated once more:

$$\sigma^{\mathrm{intra}}(\omega) = \frac{2\mathrm{i}e^2T}{\pi\hbar(\omega+\mathrm{i}\tau^{-1})}\ln\left(2\cosh\frac{\mu}{2T}\right), \tag{3}$$

where we substituted $\omega + \mathrm{i}\tau^{-1}$ for ω in order to allow for the electron relaxation τ. In this form, the intraband contribution coincides with the classical Drude–Boltzmann expression for conductivity. At low temperatures ($\mu \gg T$), when the charge carriers are degenerate, the intraband term acquires a ''metallic'' form:

$$\sigma^{\mathrm{intra}}(\omega) = \frac{\mathrm{i}e^2|\mu|}{\pi\hbar(\omega+\mathrm{i}\tau^{-1})}\,. \tag{4}$$

For pure graphene, the chemical potential is $\mu = 0$ (gapless dielectric) and conductivity (3) is proportional to the temperature. The concentration of charge carriers can be changed either by doping or by applying a constant electric field (''field effect'').

The second term in the right-hand side of Eqn (2), where δ is an infinitesimal quantity describing interband transitions, contains both a real part, which arises as a result of going around the pole and corresponds to absorption, and an imaginary part. At zero temperature, the second integral in the right-hand side of Eqn (2) can be calculated analytically as

$$\sigma^{\mathrm{inter}}(\omega) = \frac{e^2}{4\hbar}\left[\theta(\omega-2\mu) - \frac{\mathrm{i}}{2\pi}\ln\frac{(\omega+2\mu)^2}{(\omega-2\mu)^2}\right], \tag{5}$$

where θ is the step-function, which reflects the condition of interband electron transitions with the threshold $\omega = 2\mu$. The logarithmic singularity is removed by a temperature cut-off (or by relaxation of charge carriers), and at a finite but small (in comparison with the chemical potential) temperature, the following replacement should be made in (5):

$$\begin{aligned}&\theta(\omega-2\mu) \to \frac{1}{2} + \frac{1}{\pi}\arctan\left(\frac{\omega-2\mu}{2T}\right),\\ &(\omega-2\mu)^2 \to (\omega-2\mu)^2 + (2T)^2\,.\end{aligned} \tag{6}$$

The above results allow arriving at two main conclusions. First, at high frequencies $\omega \gg (T, \mu)$, the conductivity is mainly real and independent of any parameters:

$$\sigma(\omega) = \frac{e^2}{4\hbar}\,.$$

In this frequency range, which is limited from above by the band width (of about 3 eV), the conductivity, as we see, is independent of the material parameters, e.g., of the velocity v, and has a universal character. Second, if degenerate carriers exist in graphene at sufficiently low temperatures, then the imaginary part of the conductivity contains a logarithmic singularity at the threshold of the interband absorption $\omega = 2\mu$, where the real part undergoes a finite jump. This feature becomes smoothened with increasing the temperature

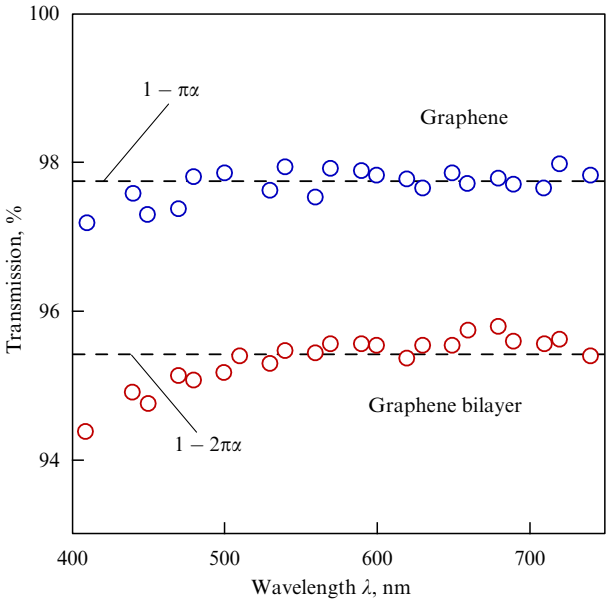

Figure 1. The coefficient of light transmission through graphene and a graphene bilayer [11].

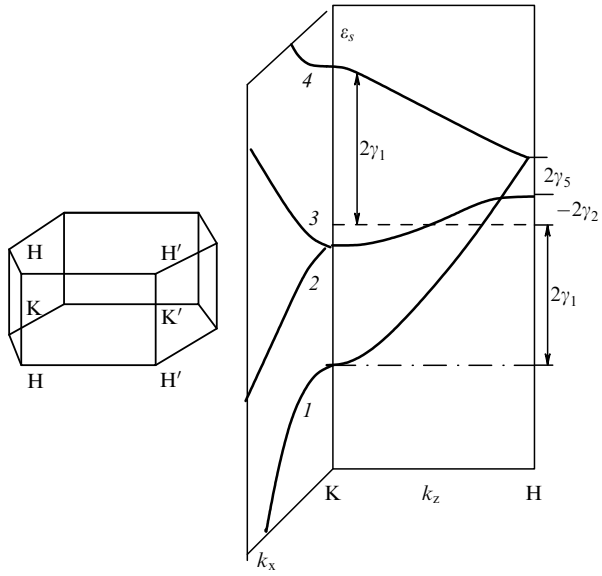

Figure 2. The Brillouin zone and the electron spectrum of graphite.

and also because of the finite length of the mean free path of charge carriers. To observe this feature, the frequency should not exceed the temperature, i.e., should be of the order of 10–40 K in energy units. These conclusions have been confirmed experimentally [8].

The universal conductivity leads to an interesting consequence. Using its value, the coefficient of transmission T of an electromagnetic wave through graphene can be obtained as [9, 10]

$$T = 1 - \frac{4\pi}{c}\,\mathrm{Re}\,\sigma(\omega)\cos\theta = 1 - \pi\,\frac{e^2}{\hbar c}\cos\theta\,, \qquad (7)$$

where θ is the incidence angle of the wave. We see that the coefficient of light transmission through a graphene layer is expressed via the fine-structure constant of quantum electrodynamics, to which graphene has no relation at all. Several experimental groups [11, 12] have confirmed the calculated value of the transmission coefficient in a wide frequency range of the visible spectrum, both for graphene and for a graphene bilayer, in which the difference of this coefficient from unity is twice greater (Fig. 1).

4. Spectrum of graphene layers in a magnetic field

The Slonczewski–Weiss Hamiltonian for a graphene bilayer and graphite in the vicinity of the KH line of the Brillouin zone has the form

$$H(\mathbf{k}) = \begin{pmatrix} \tilde\gamma_5 + U & vk_+ & \tilde\gamma_1 & \dfrac{\tilde\gamma_4 vk_-}{\gamma_0} \\ vk_- & \tilde\gamma_2 + U & \dfrac{\tilde\gamma_4 vk_-}{\gamma_0} & \dfrac{\tilde\gamma_3 vk_+}{\gamma_0} \\ \tilde\gamma_1 & \dfrac{\tilde\gamma_4 vk_+}{\gamma_0} & \tilde\gamma_5 - U & vk_- \\ \dfrac{\tilde\gamma_4 vk_+}{\gamma_0} & \dfrac{\tilde\gamma_3 vk_-}{\gamma_0} & vk_+ & \tilde\gamma_2 - U \end{pmatrix}, \qquad (8)$$

where $k_\pm = \mp \mathrm{i}k_x - k_y$ is the projection of the quasimomentum, v is the parameter of the velocity in the direction of graphite layers, $\tilde\gamma_j$ are functions of the projection k_z in the direction of the principal axis,

$$\tilde\gamma_2 = 2\gamma_2\cos(2k_z d_0)\,, \quad \tilde\gamma_5 = 2\gamma_5\cos(2k_z d_0) + \Delta\,,$$

$$\tilde\gamma_i = 2\gamma_i\cos(k_z d_0)\,, \quad i = 1, 3, 4,$$

and $d_0 = 3.35$ Å is the spacing between the layers in graphite.

The velocity parameter $v = 1.5a_0\gamma_0 = 10^8$ cm s^{-1} is related to the overlap ($\gamma_0 \approx 3$ eV) of the wave functions of nearest neighbors located in the same layer at the distance $a_0 = 1.415$ Å from each other. The parameters with $i = 1, 3, 4$, which arise because of the overlap of the wave functions of nearest neighbors in the direction of the principal axis, are an order of magnitude less than γ_0. In a bilayer, there is only one neighboring layer in the direction of the principal axis; therefore, $\tilde\gamma_i = \gamma_i$ for $i = 1, 3, 4$, and because the next layer is absent, the interlayer integrals of the overlap with the third sphere are $\tilde\gamma_i = 0$ for $i = 2, 5$, whereas they should be taken into account in graphite.

In the absence of a magnetic field, the spectrum can be computed numerically (Fig. 2) and studied analytically [13]; the specific features of conductivity related to transitions between the bands can also be studied experimentally. Hamiltonian (8) also involves the parameter U, which is important in the case of a bilayer when a constant voltage is applied to it in the direction of the principal axis. At an arbitrary value of the quasimomentum, we find four energy eigenvalues, which are numbered using subscripts $s = 1, 2, 3, 4$. At $k_x = k_y = 0$ (i.e., on the KH line) and $U = 0$, there is a twofold degeneracy ($\varepsilon_2 = \varepsilon_3$), which is a consequence of the symmetry. In an external electric field U, a gap appears in the spectrum; it is this feature that mainly accounts for the enhanced interest in bilayers. In addition, the simple quadratic behavior in the bands that touch each other acquires the shape of a Mexican hat. There is one more detail that should be taken into account: two points, K and K′, which pass into one another under rotations and

reflection ($x \to -x$), are not equivalent in the bilayer; the reflection corresponds to the permutation $k_+ \leftrightarrow k_-$ in Hamiltonian (1). To avoid the enumeration of obvious possibilities, we restrict ourselves to the description of the graphite spectrum at $U = 0$ and only then turn to a bilayer.

The problem becomes more complex and more interesting in the presence of a magnetic field. In a magnetic field B that is parallel to the principal axis, the projections of the quasi-momentum $k_{x,y}$ are operators with the commutation relation $\{\hat{k}_+, \hat{k}_-\} = -2e\hbar B/c$; it is therefore convenient to introduce creation and annihilation operators a^+ and a that change the Landau index by unity:

$$\hat{k}_+ = \sqrt{\frac{2|e|\hbar B}{c}}\, a\,, \quad \hat{k}_- = \sqrt{\frac{2|e|\hbar B}{c}}\, a^+\,.$$

For graphene, an explicit expression for the spectrum is found using Eqn (1) in the form

$$\varepsilon_{1,2} = \mp v\sqrt{\frac{2|e|\hbar B n}{c}}\,,$$

where $n = 0, 1, \ldots$.

The eigensolutions for matrix Hamiltonian (8) are sought in the form of a column,

$$\psi^{\alpha}_{sn}(x) = \begin{Bmatrix} C^1_{sn}\varphi_{n-1}(x) \\ C^2_{sn}\varphi_n(x) \\ C^3_{sn}\varphi_{n-1}(x) \\ C^4_{sn}\varphi_{n-2}(x) \end{Bmatrix}, \tag{9}$$

where $\varphi_n(x)$ are the orthogonal Hermite functions with the Landau eigenvalue $n \geqslant 0$. At a given n, the states are numbered by the band index $s = 1, 2, 3, 4$; we use the notation $|sn\rangle$ for states by counting s, as before, from below. For brevity, we omit the standard exponentials that appear in the Landau gauge and take the degeneracy in corresponding components of the quasimomentum into account only in the final results.

It is easy to see that if we neglect terms with γ_3, which lead to a trigonal warping of the spectrum, then each line of matrix Hamiltonian (8) is proportional to a certain Hermite function, which can therefore be canceled. We thus come to the problem for eigenvectors $\mathbf{C}_{sn}$ and eigenvalues

$$\begin{pmatrix} \tilde{\gamma}_5 - \varepsilon & \omega_c\sqrt{n} & \tilde{\gamma}_1 & \omega_4\sqrt{n-1} \\ \omega_c\sqrt{n} & \tilde{\gamma}_2 - \varepsilon & \omega_4\sqrt{n} & 0 \\ \tilde{\gamma}_1 & \omega_4\sqrt{n} & \tilde{\gamma}_5 - \varepsilon & \omega_c\sqrt{n-1} \\ \omega_4\sqrt{n-1} & 0 & \omega_c\sqrt{n-1} & \tilde{\gamma}_2 - \varepsilon \end{pmatrix} \begin{Bmatrix} C^1_{sn} \\ C^2_{sn} \\ C^3_{sn} \\ C^4_{sn} \end{Bmatrix} = 0\,, \tag{10}$$

where $\omega_c = v\sqrt{2|e|\hbar B/c}$, $\omega_4 = \tilde{\gamma}_4\omega_c/\gamma_0$.

We see from (9) that at $n = 0$, the eigenvector has one nonzero component, $\mathbf{C}_0 = (0, 1, 0, 0)$, and there is only one (rather than four) energy eigenvalue

$$\varepsilon(n = 0) = \tilde{\gamma}_2\,, \tag{11}$$

which depends on k_z and intersects the Fermi level such that electrons appear in the vicinity of the K point (up to the Fermi level) and holes appear in the vicinity of the H point (Fig. 3).

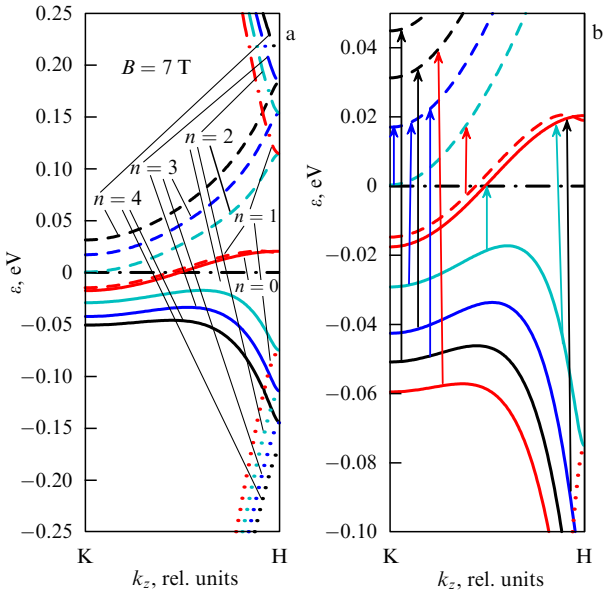

Figure 3. (Available in color online.) (a) Landau levels ε_{sn} from $n = 0$ to $n = 4$ in four bands, $s = 1, 2, 3, 4$ (dotted, solid, dashed, and dotted-and-dashed curves, respectively), depending on the projection of the momentum k_z along the KH line in the Brillouin zone of graphite ($K = 0$, $\mathrm{H} = \pi/2d_0$) for a magnetic field $B = 7$ T; the band parameters are given in the table. (b) An enlarged fragment of Fig. 3a for the bands $s = 2$ and 3.

At $n = 1$, we see from Eqns (9) that the fourth component should be set equal to zero ($C^4_{s1} = 0$), and three (rather than four) levels can be determined from the first three equations. The middle level $|21\rangle$ is very close to $|10\rangle$, and in the region of k_z where the condition $\gamma_1/\cos z \gg \gamma_2$ holds and where the electrons are located, this level has the energy

$$\varepsilon_2(n = 1) = \tilde{\gamma}_2 - 2\,\frac{\omega_c^2\,\tilde{\gamma}_4}{\tilde{\gamma}_1\gamma_0}\,. \tag{12}$$

For $n \geqslant 2$, four eigenvalues exist at any k_z. The energies of two close levels with $s = 2$ and 3 in the region $\gamma_1/\cos z \gg \gamma_2$, where electrons are located, are expressed as

$$\varepsilon_{2,3}(n) = \tilde{\gamma}_2 - \frac{\omega_c^2\,\tilde{\gamma}_4}{\tilde{\gamma}_1\gamma_0}\,(2n-1) \mp \frac{\omega_c^2}{\tilde{\gamma}_1}\,\sqrt{n(n-1)}\,. \tag{13}$$

4.1 Effect of a trigonal distortion on the spectrum in a magnetic field

In spite of the smallness of the ratio γ_3/γ_0, the effect of trigonal distortion is significant because of the degeneracy that is observed in the KH lines. To date, several ways to take the trigonal distortion into account have been suggested. Two of these are analytic: the perturbation theory [14] and semiclassical quantization [15]. The perturbation theory for the matrix Hamiltonian can suitably be constructed based on its Green's function

$$G_0^{\alpha\beta}(\varepsilon, x, x') = \sum_{sn} \frac{\psi^{\alpha}_{sn}(x)\,\psi^{*\beta}_{sn}(x')}{\varepsilon - \varepsilon_{sn}}\,, \tag{14}$$

where the superscripts can take four values, in accordance with the matrix of the Hamiltonian, and x and x' are position variables.

In the second approximation, we obtain the correction

$$\int \mathrm{d}x_1\,\mathrm{d}x_2\,G_0^{\alpha 4}(x,x_1)\,V^{42}(x_1)\,G_0^{22}(x_1,x_2)\,V^{24}(x_2)\,G_0^{4\beta}(x_2,x')\,,$$

and a similar term with the permutation of indices $2 \leftrightarrow 4$. The matrix elements of the perturbation V, labeled by the superscripts, can be easily calculated using functions (9); for the correction to the Green's function (14), we obtain the expression

$$\left(\frac{\omega_c\tilde{\gamma}_3}{\gamma_0}\right)^2 \sum_{s'sn} \frac{(n-2)|C_{sn}^4 C_{s',n-3}^2|^2 \psi_{sn}^{\alpha}(x)\,\psi_{sn}^{*\beta}(x')}{(\varepsilon-\varepsilon_{sn})(\varepsilon-\varepsilon_{s',n-3})(\varepsilon-\varepsilon_{sn})}\,. \qquad (15)$$

Correction (15) is large near the poles of the Green's function. Therefore, for ε close to ε_{sn}, we can substitute ε_{sn} in the second factor in the denominator instead of ε. Thus, the Green's function with the correction is written as

$$\frac{1}{\varepsilon-\varepsilon_{sn}} + \frac{\delta}{(\varepsilon-\varepsilon_{sn})^2}\,,$$

which, up to terms of the second order in δ, can be represented as

$$\frac{1}{\varepsilon-\varepsilon_{sn}-\delta}\,.$$

The expression obtained from (15) allows writing a correction to the eigenvalue in the form

$$\delta\varepsilon_s(n) = \left(\frac{\omega_c\tilde{\gamma}_3}{\gamma_0}\right)^2 \sum_{s'} \left[\frac{(n-2)|C_{sn}^4 C_{s',n-3}^2|^2}{\varepsilon_s(n)-\varepsilon_{s'}(n-3)} + \frac{(n+1)|C_{sn}^2 C_{s',n+3}^4|^2}{\varepsilon_s(n)-\varepsilon_{s'}(n+3)}\right], \qquad (16)$$

where the terms with $n-3<0$ can be omitted.

Formula (16) contains a parameter of the perturbation theory. We note that the spacing between the unperturbed levels can be estimated, for example, using Eqn (13). We thus find this dimensionless parameter

$$\left(\frac{\tilde{\gamma}_3\tilde{\gamma}_1}{\gamma_0\omega_c}\right)^2,$$

which turns out to be less than unity in magnetic fields $B \gg 1$ T. We also write the level $|10\rangle$ with the correction:

$$\varepsilon_1(n=0) = \tilde{\gamma}_2 + \left(\frac{\omega_c\tilde{\gamma}_3}{\gamma_0}\right)^2 \sum_{s'} \frac{|C_{s'3}^4|^2}{\tilde{\gamma}_2-\varepsilon_{s'}(3)}\,. \qquad (17)$$

The band structure in a magnetic field is shown in Fig. 3. A comparison shows that our expressions (16) and (17) for the levels give the same results as the numerical method of truncating an infinite-rank matrix [16]. We note that the expressions obtained are also applicable to a bilayer; we only should set $\gamma_2=\gamma_5=0$ and $\tilde{\gamma}_i=\gamma_i$ for $i=1, 3, 4$ and take the field U into account.

The semiclassical quantization, which we do not describe here, can suitably be introduced in the case of weak magnetic fields and relatively pure materials with a small frequency of collisions, when the observation of quantum oscillations is still possible.

5. Transmission coefficient and the magnetooptical effect in graphene layers

In the presence of a magnetic field, a radically new phenomenon is the appearance of the Hall component of conductivity, which is usually denoted by $\sigma_{xy}(\omega)$. The Hall conductivity violates the rotation symmetry about the principal axis, which leads to Faraday and Kerr effects, i.e., to the rotation of the polarization plane of light during its transmission and reflection. Electron transitions then become possible, both between band states s and between different Landau levels n; therefore, resonance denominators $\Delta_{ss'n}=\varepsilon_{sn}-\varepsilon_{s',n+1}$ appear. The method for calculating the correlator that determines the current and is expressed through the product of two Green's functions remains essentially the same as in the absence of a magnetic field.

The calculations in [13] lead to the following expressions for the two components of conductivity of graphite in the collisionless case, where the frequency of collisions Γ is much less than the spacing between the levels:

$$\left\{\begin{matrix}\sigma_{xx}(\omega)\\ \mathrm{i}\sigma_{xy}(\omega)\end{matrix}\right\} = \mathrm{i}\sigma_0\,\frac{4\omega_c^2}{\pi^2}\sum_{n,s,s'}\int_0^{\pi/2}\mathrm{d}z\,\frac{\Delta f_{ss'n}}{\Delta_{ss'n}}\,|\mathrm{d}_{ss'n}|^2 \times\left[(\omega+\mathrm{i}\Gamma+\Delta_{ss'n})^{-1}\pm(\omega+\mathrm{i}\Gamma-\Delta_{ss'n})^{-1}\right], \qquad (18)$$

where the integration is performed over one-half of the Brillouin zone, $0<z<\pi/2$; in the case of graphene and a bilayer, it is not performed. Here, $\Delta f_{ss'n}=f(\varepsilon_{s'n+1})-f(\varepsilon_{sn})$ is the difference of distribution functions with the shift of levels due to trigonal distortion taken into account, and the matrix element of the dipole moment

$$d_{ss'n}=C_{sn}^2C_{s'n+1}^1+C_{sn}^3C_{s'n+1}^4+\frac{\tilde{\gamma}_4}{\gamma_0}\,(C_{sn}^1C_{s'n+1}^4+C_{sn}^2C_{s'n+1}^3)$$

is expressed in terms of the components of wave function (9). The most intense electron transitions that are taken into account satisfy the selection rule $\Delta n=1$.

In addition, the renormalization of the dipole moment, in other words, of the electron–photon vertex, due to the trigonal distortion must be taken into account. This renormalization leads to additional weak lines, obtained by replacing the matrix element in (18) by the quantity

$$d_{ss'n}=\frac{\tilde{\gamma}_3}{\gamma_0}\,C_{sn}^2C_{s'n+2}^4$$

and by the replacement $n+1\to n+2$ with the new selection rule $\Delta n=2$.

The results of calculations are shown in Figs 4 and 5. The Kerr rotation angle reaches giant values, which exceed the values typical of semiconductors by more than an order of magnitude. The oscillations of the angle are related to certain electron transitions, and the position of its maxima (as well as of reflection minima) are determined either by the boundaries of the Landau levels at the K and H points or by the intersection of these levels with the Fermi level (Fig. 3b). We note that the dispersion of the levels affects the positions of optical features. We used the parameters of Hamiltonian (8) presented in the table. Their values (also see [19, 20]) differ from those obtained in various experimental studies only because we took a different form of the Hamiltonian than the one used by Slonczewski and Weiss (the third line of the

Table. Parameters of Hamiltonian (8), their relation to the Slonczewski–Weiss (SW) notation, and the numerical values (in meV) obtained in experimental work [17, 18].

Hamiltonian (8)	γ_0	γ_1	γ_2	γ_3	γ_4	γ_5	Δ	ε_F
	3050	360	−10.2	270	−150	−1.5	16	−4.1
SW [1]	γ_0	γ_1	$2\gamma_2$	γ_3	$-\gamma_4$	$2\gamma_5$	$\Delta + 2(\gamma_2 - \gamma_5)$	$2\gamma_2 + \varepsilon_F$
Mendez et al. [17]	3160	390	− 20	276	44	38	8	−24
Doezema et al. [18]	3120	380	−21	315	120	−3	−2	—

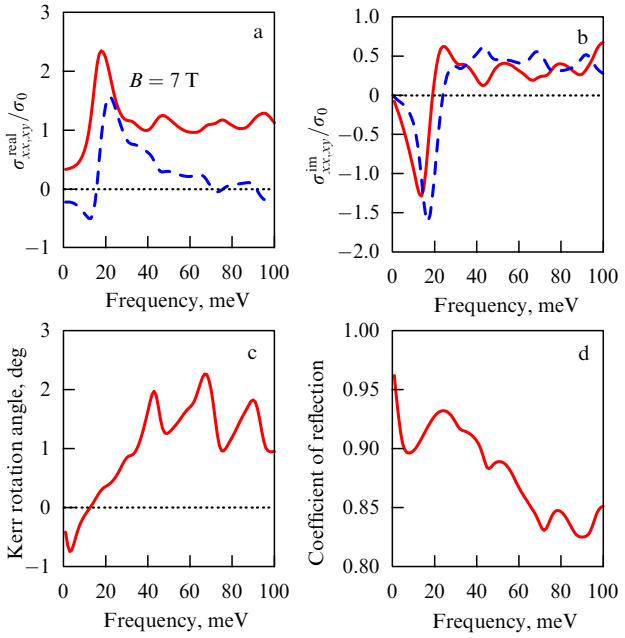

Figure 4. (a) Real and (b) imaginary parts of the longitudinal (xx), solid curve, and Hall (xy), dashed curve, dynamic conductivity of graphite. (c) Kerr rotation angle and (d) reflection coefficient in the magnetic field $B = 7$ T at the temperature $T = 0.1$ meV; the electronic relaxation frequency is $\Gamma = 3.5$ meV.

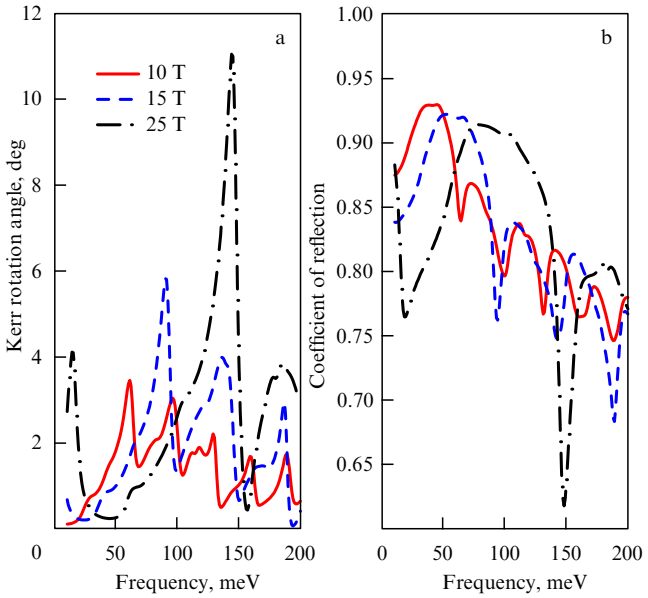

Figure 5. (a) Kerr rotation angle and (b) reflection coefficient of graphite in strong magnetic fields (10, 15, and 25 T) depending on the frequency of the electromagnetic wave.

table). The experimental values of the parameters γ_4, γ_5, and Δ exhibit a significant scatter; our values are close to those obtained in [17]. We note that in strong magnetic fields, the Fermi level increases to $\varepsilon_F \approx -1$ meV from the value given in the table for weak fields.

6. Conclusion

To the best of our knowledge, measurements of the Kerr and Faraday rotation angles in graphene layers have been made only at the University of Geneva, and we are grateful to A Kuzmenko and J Levallois for the fruitful discussions and for the opportunity to become acquainted with the experimental results before they were published.

Acknowledgments. This work was supported in part by the Russian Foundation for Basic Research (project No. 10-02-00193-a), by the National Research Foundation of Sweden (grant no. Scopes IZ73Z0_128026), and by the SIMTECH Program, New Century of Superconductivity: Ideas, Materials and Technologies (grant no. 246937).

References

1. Slonczewski J C, Weiss P R *Phys. Rev.* **109** 272 (1958)
2. Elias D C et al. *Nature Phys.* **7** 701 (2011)
3. Abrikosov A A, Beneslavskii S D *Zh. Eksp. Teor. Fiz.* **59** 1280 (1970) [*Sov. Phys. JETP* **32** 699 (1971)]
4. Mishchenko E G *Phys. Rev. Lett.* **98** 216801 (2007)
5. Falkovsky L A, Varlamov A A *Eur. Phys. J. B* **56** 281 (2007)
6. Gusynin V P, Sharapov S G, Carbotte J P *Phys. Rev. Lett.* **96** 256802 (2006)
7. Gusynin V P, Sharapov S G, Carbotte J P *Phys. Rev. B* **75** 165407 (2007)
8. Li Z Q et al. *Nature Phys.* **4** 532 (2008)
9. Falkovsky L A, Pershoguba S S *Phys. Rev. B* **76** 153410 (2007)
10. Kuzmenko A B et al. *Phys. Rev. Lett.* **100** 117401 (2008)
11. Nair R R et al. *Science* **320** 1308 (2008)
12. Mak K F et al. *Phys. Rev. Lett.* **101** 196405 (2008)
13. Falkovsky L A *Phys. Rev. B* **82** 073103 (2010)
14. Falkovsky L A *Zh. Eksp. Teor. Fiz.* **94** 783 (2011) [*JETP Lett.* **94** 723 (2011)]
15. Ozerin A Yu, Falkovsky L A, arXiv:1203.0157
16. Nakao K *J. Phys. Soc. Jpn.* **40** 761 (1976)
17. Doezema R E et al. *Phys. Rev. B* **19** 4224 (1979)
18. Mendez E, Misu A, Dresselhaus M S *Phys. Rev. B* **21** 827 (1980)
19. Kuzmenko A B et al. *Phys. Rev. B* **80** 165406 (2009)
20. Brandt N B, Chudinov S M, Ponomarev Ya G *Semimetals I. Graphite and its Compounds* (Amsterdam: Elsevier, 1988)
21. Crassee I et al. *Nature Phys.* **7** 48 (2011)